Shape Resonances in Silane and Fluorinated silanes

Hrishikesh Rajbongshi, Deepak Kumar, Mwdansar Banuary, and Ashish Kumar Gupta*

Department of Chemistry, Indian Institute of Technology Guwahati, Assam, India

E-mail: gupta@iitg.ac.in

Supporting Information

BOX CAP optimization

The CAP is highly dependent on the scaling parameter and the dimensions of the box potential. While the optimal scaling parameter can be determined graphically, the main challenge is to determine the optimal dimensions of the box potential.

The method for finding the optimized parameters of the additional potential is outlined step by step for the silane (SiH_4) molecule.

A cubic box with approximate dimensions is selected as the starting point for the analysis. The dimensions of this approximate box are determined based on chemical intuition. Since the Si-H bond length is 1.5 Å, a cubic box with x_0=y_0=z_0=4.23 Å=8.0 a.u., is chosen as the initial setup, and the following process is described below in a step-wise manner.

a) An η trajectory calculation is carried out using the cc-pVDZ+5p basis set. This η-trajectory contains multiple cusps corresponding to the resonance state and continuum states.

b) The cusp regarding the resonance state among the sea of continuum states is obtained using the nuclear charge stabilization method in conjunction with PEM. The cusp regarding the true LUMO is shown in Figure 1.

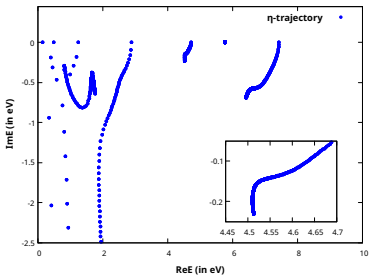

Figure 1: The η-trajectory for SiH_4, obtained using cc-pVDZ+5p basis set shows multiple cusps. The resonance state is shown in the inset, which is identified via the NCS-PEM calculations. The additional nuclear charge is added to the central Si atom only.

c) The next step is to find out how the resonance energy varies with respect to the change in the size of the cubic box. For this purpose, an x_0 trajectory calculation is carried out at the η_{opt} obtained in the previous step. Since a cubic box is considered, x_0, y_0, and z_0 are equal,

and the trajectory is defined as cubic trajectory. At the optimal cubic box, the change in resonance energy with respect to changes in the box parameter is minimal. The optimal size of the box can be obtained from the cubic trajectory by looking at the cusp corresponding to the resonance state. The cusp in Figure 2, corresponds to value of x_0=y_0=z_0=7.50 a.u..

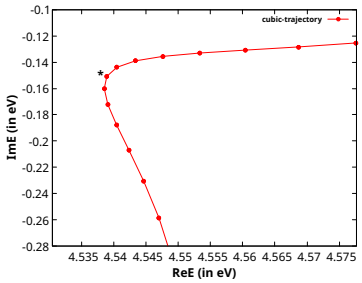

Figure 2: The x_0-trajectory for SiH_4 with cc-pVDZ+5p basis set;for x_0=y_0=z_0. The stabilization point is shown by an asterisk.

d) Some additional calculations are carried out to check the effect of cuboid box potentials on the resonance energy. This time, the y_0 and z_0 values are set equal to the optimized cubic box parameter (i.e. 7.50 a.u.) and only the x_0 value is varied. This gives a series of eigenvalues for different cuboid box potentials where $x_0 \neq y_0$=z_0=7.50 a.u.. This is defined as x-cuboid trajectory calculation. Similarly, y-cuboid and z-cuboid trajectory calculations are performed.

e) The cusps corresponding to the cuboid trajectories are inseparable from the cusp of the cubic trajectory. This indicates that the change in symmetry of the optimized cubic box has a minimal impact on the resonance energy value. The optimized cubic box is used for further calculations.

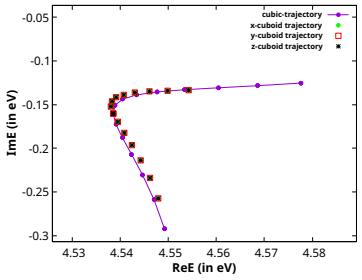

Figure 3: Comparison between the stabilization points obtained from cubic(x_0=y_0=z_0) potential and x-,y- and z-cuboid potentials.

Thus, the optimized dimensions of the box CAP for SiH_4 is x_0=y_0=z_0=7.50 a.u..

The Procedure for basis set selection

The basis sets for the calculations are selected using a systematic convergence strategy. The process starts with the cc-pVDZ basis set, to which additional diffuse functions (s-type, p-type, and d-type) are incrementally added until convergence of both the resonance position and width is achieved.

For larger basis sets, such as aug-cc-pVDZ and cc-pVTZ, the augmentation pattern established for the converged cc-pVDZ basis set is retained. Since cc-pVDZ and aug-cc-pVDZ bases obtained from the Basis set exchange library do not include f-type functions, no additional f-type functions are considered in these cases. However, the cc-pVTZ basis set already contains f-type functions; therefore, additional diffuse f-type functions are also introduced alongside s-type, p-type, and d-type functions.

For example, in the case of SiH_4, starting from the cc-pVDZ basis set, convergence of the resonance energy was achieved upon inclusion of five additional p-type and five d-type functions (*i.e.* cc-pVDZ+5p5d), while the s-type diffuse functions had a negligible effect. Since the aug-cc-pVDZ basis set already includes one diffuse function of each angular momentum compared to cc-pVDZ, the augmentation pattern is preserved by adding +4p4d, rather than +5p5d diffuse functions. Accordingly, calculations were performed using aug-cc-pVDZ+4p4d, aug-cc-pVDZ+5p4d, and cc-pVTZ+5p4d basis sets. For the cc-pVTZ basis set, additional diffuse f-type functions (four and five) were also introduced to analyse their impact on the resonance energy.

Silane,SiH_4

Cartesian coordinates in Angstroms

	X	Y	Z
Si	0.0000	0.0000	0.0000
H	0.8544	0.8544	0.8544
H	-0.8544	-0.8544	0.8544
H	-0.8544	0.8544	-0.8544
H	0.8544	-0.8544	-0.8544

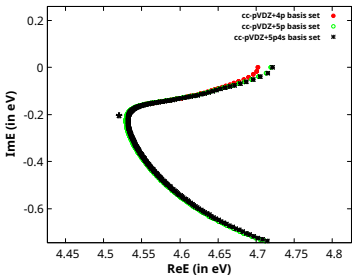

Figure 4: η-trajectories for the resonance state of SiH_4 with cc-pVDZ+4p, cc-pVDZ+5p and cc-pVDZ+5p4s basis sets.

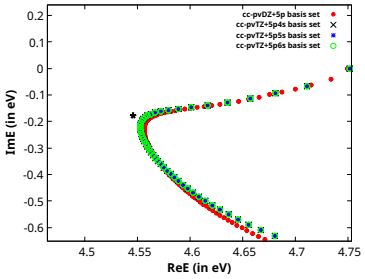

Figure 5: The η-trajectories for the resonance state of SiH_4 with various basis sets. It can be seen that the additional s-type functions to the basis set do not affect the resonance energy.

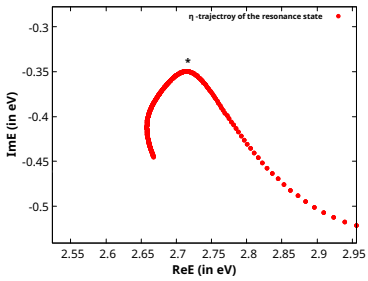

Figure 6: η-trajectories for the resonance state of SiH_4 with cc-pVDZ+5p4d basis sets.

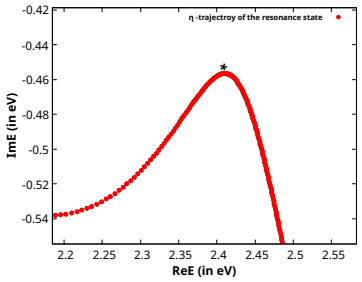

Figure 7: η-trajectories for the resonance state of SiH_4 with aug-cc-pVDZ+4p4d basis sets.

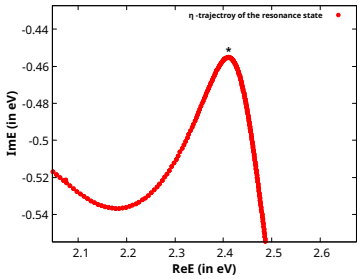

Figure 8: η-trajectories for the resonance state of SiH_4 with aug-cc-pVDZ+5p4d basis sets.

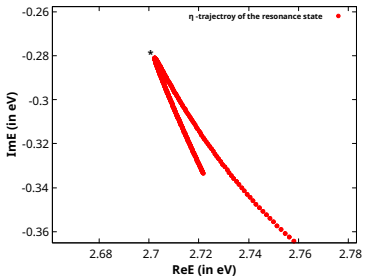

Figure 9: η-trajectories for the resonance state of SiH_4 with cc-pVTZ+5p4d basis sets.

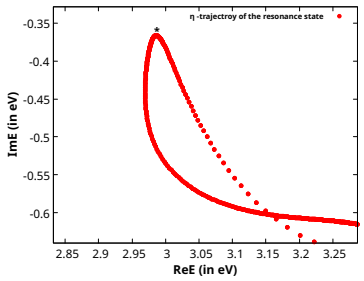

Figure 10: η-trajectories for the resonance state of SiH_4 with cc-pVTZ+5p4d4f basis sets.

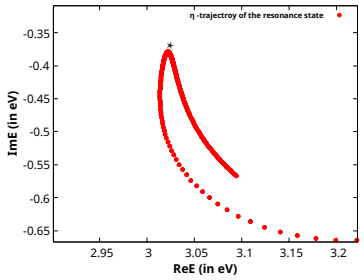

Figure 11: η-trajectories for the resonance state of SiH_4 with cc-pVTZ+5p4d5f basis sets.

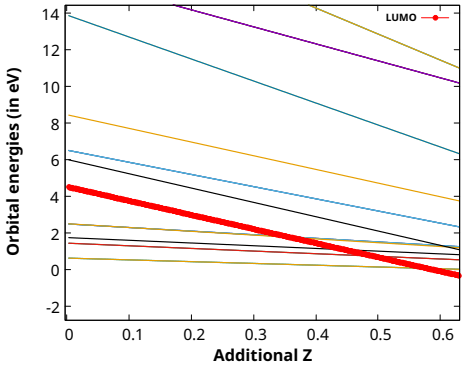

Figure 12: NCS-PEM plot of SiH_4 with cc-pVDZ+5p4s basis set.

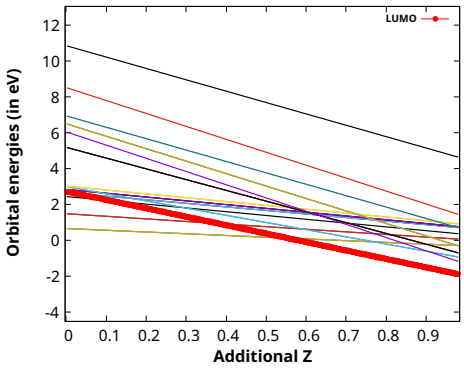

Figure 13: NCS-PEM plot of SiH_4 with cc-pVDZ+5p4d basis set.

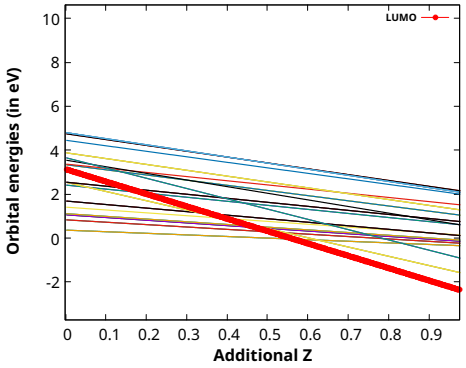

Figure 14: NCS-PEM plot of SiH_4 with aug-cc-pVDZ+5p4d basis set.

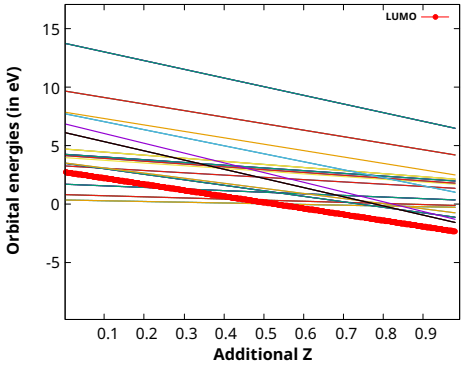

Figure 15: NCS-PEM plot of SiH_4 with cc-pVTZ+5p4d basis set.

Fluorosilane,SiH_3F

Cartesian coordinates in Angstroms

	X	Y	Z
Si	0.0000	0.0000	0.4986
F	0.0000	0.0000	-1.0959
H	0.0000	1.4017	0.9613
H	-1.2139	-0.7008	0.9613
H	1.2139	-0.7008	0.9613

Difluorosilane,SiH_2F_2

Cartesian coordinates in Angstroms

	X	Y	Z
Si	0.0000	0.0000	0.4452
F	0.0000	1.2731	-0.4835
F	0.0000	-1.2731	-0.4835
H	1.2297	0.0000	1.2351
H	-1.2297	0.0000	1.2351

Trifluorosilane,$SiHF_3$

Cartesian coordinates in Angstroms

	X	Y	Z
Si	0.0000	0.0000	0.3204
F	0.0000	1.4619	-0.2317
F	1.2660	-0.7309	-0.2317
F	-1.2660	-0.7309	-0.2317
H	0.0000	0.0000	1.7691

Tetraflurosilane,SiF_4

Cartesian coordinates in Angstroms

	X	Y	Z
Si	0.0000	0.0000	0.0000
F	0.8972	0.8972	0.8972
F	-0.8972	-0.8972	0.8972
F	-0.8972	0.8972	-0.8972
F	0.8972	-0.8972	-0.8972

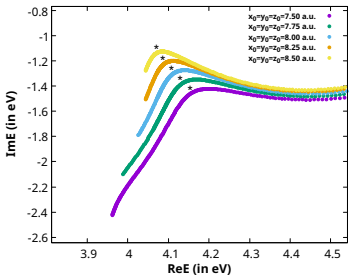

Figure 16: η-trajectories for the resonance state of SiF_4 obtained at different box sizes. The calculations were performed at HF/cc-pVDZ+7s level. The resonance energy does not change significantly. Therefore, the cubic box potential that was optimized for SiH_4 is utilized for all the molecules in this study.

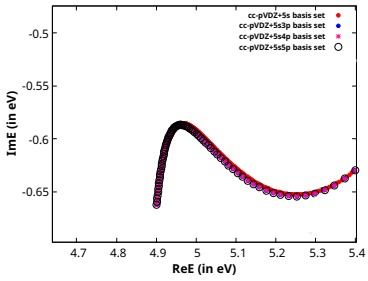

Figure 17: The η-trajectories for the resonance state of SiF_4 with various basis sets. It can be seen that the additional p-type functions to the basis set do not affect the resonance energy.

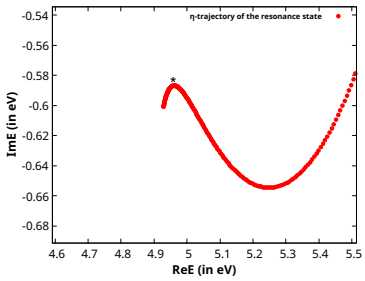

Figure 18: η-trajectory for the resonance state of SiF_4 with cc-pVDZ+5s5p basis set.

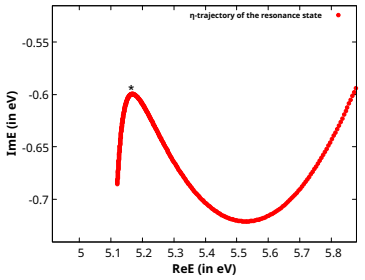

Figure 19: η-trajectory for the resonance state of SiF_4 with cc-pVDZ+5s6d basis set.

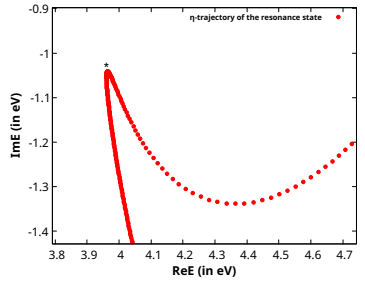

Figure 20: η-trajectory for the resonance state of SiF_4 with cc-pVTZ+5s6d basis set.

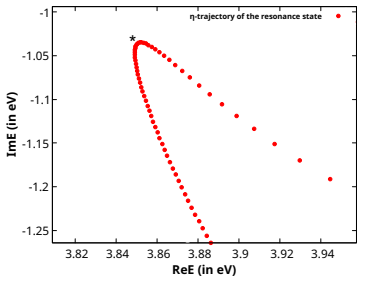

Figure 21: η-trajectory for the resonance state of SiF_4 with cc-pVTZ+5s6d basis set.

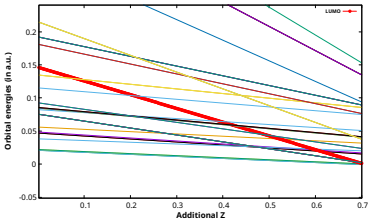

Figure 22: NCS-PEM plot of SiF_4 with cc-pVTZ+5s6d basis set.

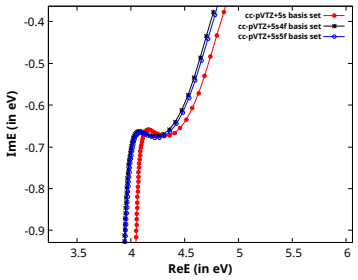

Figure 23: η-trajectories of the resonance state of SiF_4 for cc-pVTZ+5s/5s4f/5s5f basis sets. The results show minimal effect of the additional f-type functions.

CAP/ToDEP calculations

Table 1: Comparison between the resonance energies for SiH_4 using SoDEP and ToDEP calculations.

Basis set	SoDEP		ToDEP	
	Resonance position (eV)	Width (eV)	Resonance position (eV)	Width (eV)
cc-pVDZ+3p	0.16	0.07	0.17	0.07
cc-pVDZ+4p	0.16	0.09	0.17	0.08

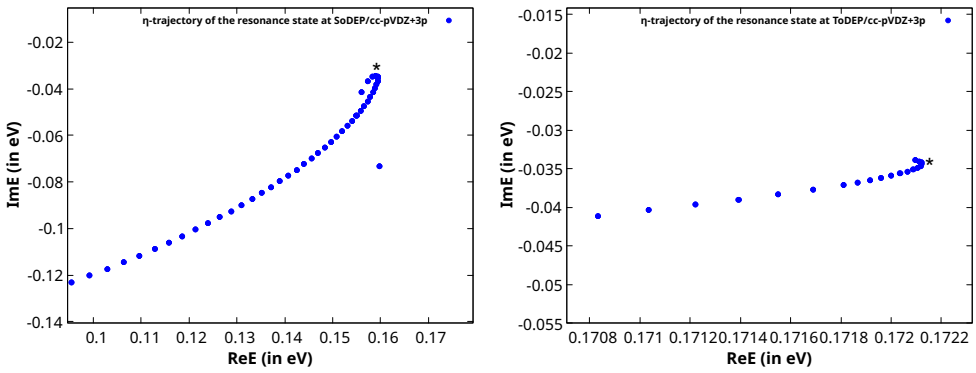

(a) (b)

Figure 24: a) η-trajectory of the resonance state at SoDEP/cc-pVDZ+3p level; b) η-trajectory corresponding to resonance state at ToDEP/cc-pVDZ+3p level.

Basis Set Dependence of Resonance Energies at the SoDEP Level

The SoDEP approach introduces correlation and relaxation effects beyond the Hartree–Fock description. In our study, we achieved basis-set convergence at the HF level and used that basis set to calculate the SoDEP energy. For SoDEP calculations, the converged C-matrix at the HF-level is used. Consequently, the influence of diffuse functions, which primarily determine the description of the continuum-like resonance state at the HF level, is expected to be largely retained at the SoDEP level.

To verify this, additional SoDEP calculations for SiH_4 were performed using different augmented basis sets. The effect of diffuse functions of different angular momenta was found to be similar to their effect at the HF level. For example, at HF-level, the s-type functions had no effect on the resonance energy of SiH_4, and the same behaviour is observed in the SoDEP level. The results are presented in Table 2. The corresponding η-trajectories are shown in Figure 25. For the η-trajectories shown in black, to save computational effort, the calculation is performed only around the cusp, rather than from η=0.

Table 2: The variation of resonance energies with different basis sets at the SoDEP level of theory. The effect of additional diffuse functions with different angular momenta is the same as in the HF-level.

Basis set	Resonance energy (eV)	
	Position	Width
cc-pVDZ+4p	3.97	0.16
cc-pVDZ+5p	3.98	0.17
cc-pVDZ+5p4s	3.97	0.18
cc-pVDZ+5p5s	3.97	0.18
cc-pVDZ+5p6s	3.97	0.18
cc-pVDZ+5p4d	2.49	0.57
cc-pVDZ+5p5d	2.51	0.63
cc-pVTZ+5p4d4f	2.60	0.68
cc-pVTZ+5p4d5f	2.63	0.70

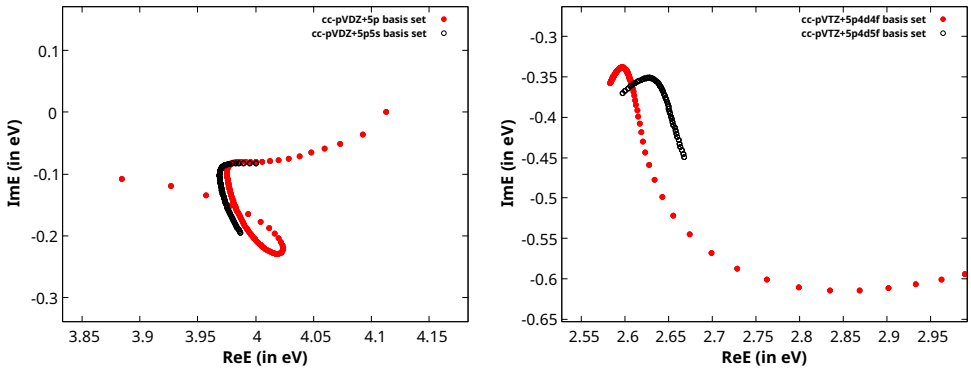

(a) (b)

Figure 25: η-trajectories of the resonance state of SiH_4.

Additionally, for the other molecules, basis set convergence of the reported SoDEP results was verified by targeted augmentation of the employed basis set. For example, in the case of SiF_4, the result reported in the manuscript was at the SoDEP/cc-pVTZ+5s6d level, so an additional calculation was performed with an expanded cc-pVTZ+5s7d basis set. The resulting SoDEP energies showed marginal variation. This confirms that the reported values are well converged with respect to the basis set size. Similar calculations were performed for the other molecules (SiH_3F, SiH_2F_2, and $SiHF_3$). The results are given in Table 3 and the corresponding η-trajectories are shown in Figure 26 and 27. For the η-trajectories shown in

black , to save computational effort, the calculation is done only around the cusp, rather than from η=0.

Table 3: Resonance energies for different molecules with various basis sets at the SoDEP level of theory.

Molecule	Basis set	Resonance energy(in eV)
SiH_3F	cc-pVTZ+5p4s6d4f	2.72(0.71)
	cc-pVTZ+5p5s5d5f	2.73(0.71)
SiH_2F_2	cc-pVTZ+5p5s4d4f	2.88(1.14)
	cc-pVTZ+5p5s5d5f	2.87(1.13)
$SiHF_3$	cc-pVTZ+5p4s5d4f	3.21(1.58)
	cc-pVTZ+5p4s6d4f	3.27(1.57)
SiF_4	cc-pVTZ+5s6d	3.43(1.86)
	cc-pVTZ+5s7d	3.58(1.89)

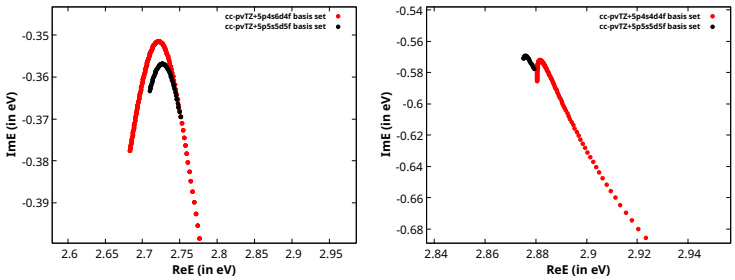

(a) (b)

Figure 26: η-trajectories of the resonance state of (a) SiH_3F and (b)SiH_2F_2 at SoDEP level.

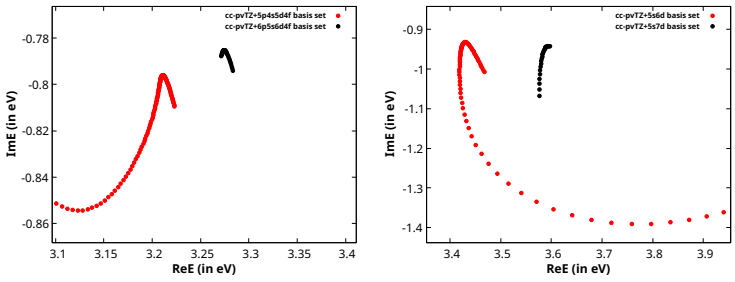

(a) (b)

Figure 27: η-trajectories of the resonance state of (a) $SiHF_3$ and (b)SiF_4 at SoDEP level.

These results confirm that the chosen basis sets provide a consistent and reliable description of the resonance states at both HF and SoDEP levels.

Consistency of the calculated results with experimental results

The reported resonance energies have significant deviations from the experimental results. In particular, the resonance width for SiH_4 has an error of 32%. However, it is important to note that the percentage error of this magnitude is common in the theoretical study of shape resonance. We have mentioned some recent studies (Tables 4 and 5), where the final results show a similar percentage of error.

Table 4: Comparison of reported and experimental resonance energies for N_2.

N_2^- shape resonance				
	position(eV)	% error	width(eV)	% error
Experimental[1]	2.32	-	0.41	-
CAP-EOM-EA-CCSD[2]	2.75	18.5	0.26	36
EOM-EA-CCSD[3]	2.54	8.6	0.52	26
CAP/PP-CASSCF[4]	3.83	65	0.25	39

Table 5: Comparison of reported and experimental resonance energies for CO.

CO^- shape resonance				
	position(eV)	% error	width(eV)	% error
Experimental[5]	1.50	-	0.40	-
CAP-EOM-EA-CCSD[6]	2.09	39	0.61	48
EOM-EA-CCSD[3]	2.04	36	1.03	157

In conclusion, it can be said that,

- Although the range of percentage error in the reported energies is fairly common, the term 'closely align' may refer to a very small percentage error (less than 1.0%).
- For SiF_4, the experimental value range is broad. Even so, we maintain that our calculated values are within reasonable alignment with those results.

Hence, in the manuscript, we have mentioned that the computed results are reasonably consistent with the experimental values.

References

(1) Berman, M.; Estrada, H.; Cederbaum, L. S.; Domcke, W. Nuclear dynamics in resonant electron-molecule scattering beyond the local approximation: The 2.3-eV shape resonance in N 2. *Physical Review A* **1983**, *28*, 1363.

(2) Zuev, D.; Jagau, T.-C.; Bravaya, K. B.; Epifanovsky, E.; Shao, Y.; Sundstrom, E.; Head-Gordon, M.; Krylov, A. I. Complex absorbing potentials within EOM-CC family of methods: Theory, implementation, and benchmarks. *The Journal of chemical physics* **2014**, *141*.

(3) White, A. F.; Epifanovsky, E.; McCurdy, C. W.; Head-Gordon, M. Second order Møller-Plesset and coupled cluster singles and doubles methods with complex basis functions for resonances in electron-molecule scattering. *The Journal of Chemical Physics* **2017**, *146*.

(4) Das, S.; Samanta, K. Investigation of electron-induced scattering resonances using a multiconfigurational polarization propagator and a complex absorbing potential. *Chemical Physics* **2023**, *564*, 111712.

(5) Ehrhardt, H.; Langhans, L.; Linder, F.; Taylor, H. Resonance scattering of slow electrons from H 2 and CO angular distributions. *Physical Review* **1968**, *173*, 222.

(6) Landau, A.; Moiseyev, N. Molecular resonances by removing complex absorbing potentials via Padé; Application to CO- and N 2-. *The Journal of Chemical Physics* **2016**, *145*.